J|A|C|S
ARTICLES
Published on Web 09/03/2005

Structural Basis for the Enantioselectivity of an Epoxide Ring Opening Reaction Catalyzed by Halo Alcohol Dehalogenase HheC

René M. de Jong,[†] Jan J. W. Tiesinga,[†] Alessandra Villa,[†] Lixia Tang,[‡] Dick B. Janssen,[‡] and Bauke W. Dijkstra*,[†]

Contribution from the Departments of Biophysical Chemistry and Biochemistry, Groningen Biomolecular Sciences and Biotechnology Institute, University of Groningen, Nijenborgh 4, NL-9747 AG, Groningen, The Netherlands

Received May 15, 2005; E-mail: B.W.Dijkstra@rug.nl

Abstract: Halo alcohol dehalogenase HheC catalyzes the highly enantioselective dehalogenation of vicinal halo alcohols to epoxides, as well as the reverse reaction, the enantioselective and β-regioselective nucleophilic ring opening of epoxides by pseudo-halides such as azide and cyanide. To investigate this latter reaction, we determined X-ray structures of complexes of HheC with the favored and unfavored enantiomers of *para*-nitrostyrene oxide. The aromatic parts of the two enantiomers bind in a very similar way, but the epoxide ring of the unfavored (*S*)-enantiomer binds in a nonproductive inverted manner, with the epoxide oxygen and Cβ atom positions interchanged with respect to those of the favored (*R*)-enantiomer. The calculated difference in relative Gibbs binding energy is in agreement with the observed loss of a single hydrogen bond in the *S* bound state with respect to the *R* bound state. Our results indicate that it is the nonproductive binding of the unfavored (*S*)-enantiomer, rather than the difference in affinity for the two enantiomers, that allows HheC to catalyze the azide-mediated ring opening of *para*-nitrostyrene oxide with high enantioselectivity. This work represents a rare opportunity to explain the enantioselectivity of an enzymatic reaction by comparison of crystallographic data on the binding of both the favored and unfavored enantiomers.

Introduction

Enzymes such as lipases and esterases are frequently used for the synthesis of optically pure compounds, and various efforts have been made to explain, predict, and improve their selectivity.[1−3] Also, new enzymes for biotransformations that yield enantiopure compounds continue to be reported.[4] Halo alcohol dehalogenase HheC from *Agrobacterium radiobacter* AD1 is a potentially useful enzyme for catalyzing enantioselective conversions under mild conditions.[5,6] The enzyme catalyzes the dehalogenation of various aliphatic and aromatic vicinal halo alcohols, such as 1,3-dichloro-2-propanol and 2-phenyl-1-chloro-2-ethanol, producing HCl and the corresponding epoxides. X-ray structures of HheC in complex with a halo alcohol mimic and with dehalogenation products have provided structural insight into its catalytic mechanism.[7] The vicinal halo alcohol substrate binds near a Ser132-Tyr145-Arg149 catalytic triad, with its hydroxyl group interacting with Ser132 and Tyr145 of the triad. The halogen is bound in a halide-binding site (Figure 1A,B). Tyr145 activates the hydroxyl group of the substrate, allowing the S_N2-type intramolecular substitution of the halogen atom by the hydroxyl oxygen atom (Figure 1C). The pK_a of Tyr145 is decreased by Arg149, which also relays the abstracted proton via two buried water molecules to the partly solvent-exposed Asp80.

The halide-binding site of HheC can also accommodate other small negatively charged ions such as azide, cyanide, and nitrite. These ions can replace the halide ion in the reverse reaction, the enantioselective and β-regioselective nucleophilic ring opening of epoxides (Figure 1D).[8−11] This ring opening reaction requires acidic conditions (pH 4−5) that allow the tyrosine to protonate a bound epoxide substrate,[10] while the anionic nucleophile attacks the Cβ atom of the epoxide ring, producing the corresponding β-substituted alcohol.

Kinetic analysis of the dehalogenation of racemic *para*-nitro-2-bromo-1-phenylethanol (pNSHH) showed that the high enantioselectivity of HheC toward this substrate ($E = 150$) depends

[†] Department of Biophysical Chemistry.
[‡] Department of Biochemistry.

(1) Kazlauskas, R. J. *Curr. Opin. Chem. Biol.* **2000**, *4*, 81−88.
(2) Bornscheuer, U. T. *Curr. Opin. Biotechnol.* **2002**, *13*, 543−547.
(3) Reetz, M. T. *Proc. Natl. Acad. Sci. U.S.A.* **2004**, *101*, 5716−5722.
(4) Faber, K.; Kroutil, W. *Curr. Opin. Chem. Biol.* **2005**, *9*, 181−187.
(5) van Hylckama Vlieg, J. E. T.; Tang, L.; Lutje Spelberg, J. H.; Smilda, T.; Poelarends, G. J.; Bosma, T.; van Merode, A. E. J.; Fraaije, M. W.; Janssen, D. B. *J. Bacteriol.* **2001**, *183*, 5058−5066.
(6) de Vries, E. J.; Janssen, D. B. *Curr. Opin. Biotechnol.* **2003**, *14*, 414−420.
(7) de Jong, R. M.; Tiesinga, J. J. W.; Rozeboom, H. J.; Kalk, K. H.; Tang, L.; Janssen, D. B.; Dijkstra, B. W. *EMBO J.* **2003**, *22*, 4933−4944.
(8) Lutje Spelberg, J. H.; van Hylckama Vlieg, J. E. T.; Tang, L.; Janssen, D. B.; Kellogg, R. M. *Org. Lett.* **2001**, *3*, 41−43.
(9) Lutje Spelberg, J. H.; Tang, L.; van Gelder, M.; Kellogg, R. M.; Janssen, D. B. *Tetrahedron: Asymmetry* **2002**, *13*, 1083−1089.
(10) Lutje Spelberg, J. H.; Tang, L.; Kellogg, R. M.; Janssen, D. B. *Tetrahedron: Asymmetry* **2004**, *15*, 1095−1102.
(11) Hasnaoui, G.; Lutje Spelberg, J. H.; de Vries, E.; Tang, L.; Hauer, B.; Janssen, D. B. *Tetrahedron: Asymmetry* **2004**, *15*, 1095−1102.

10.1021/ja0531733 CCC: $30.25

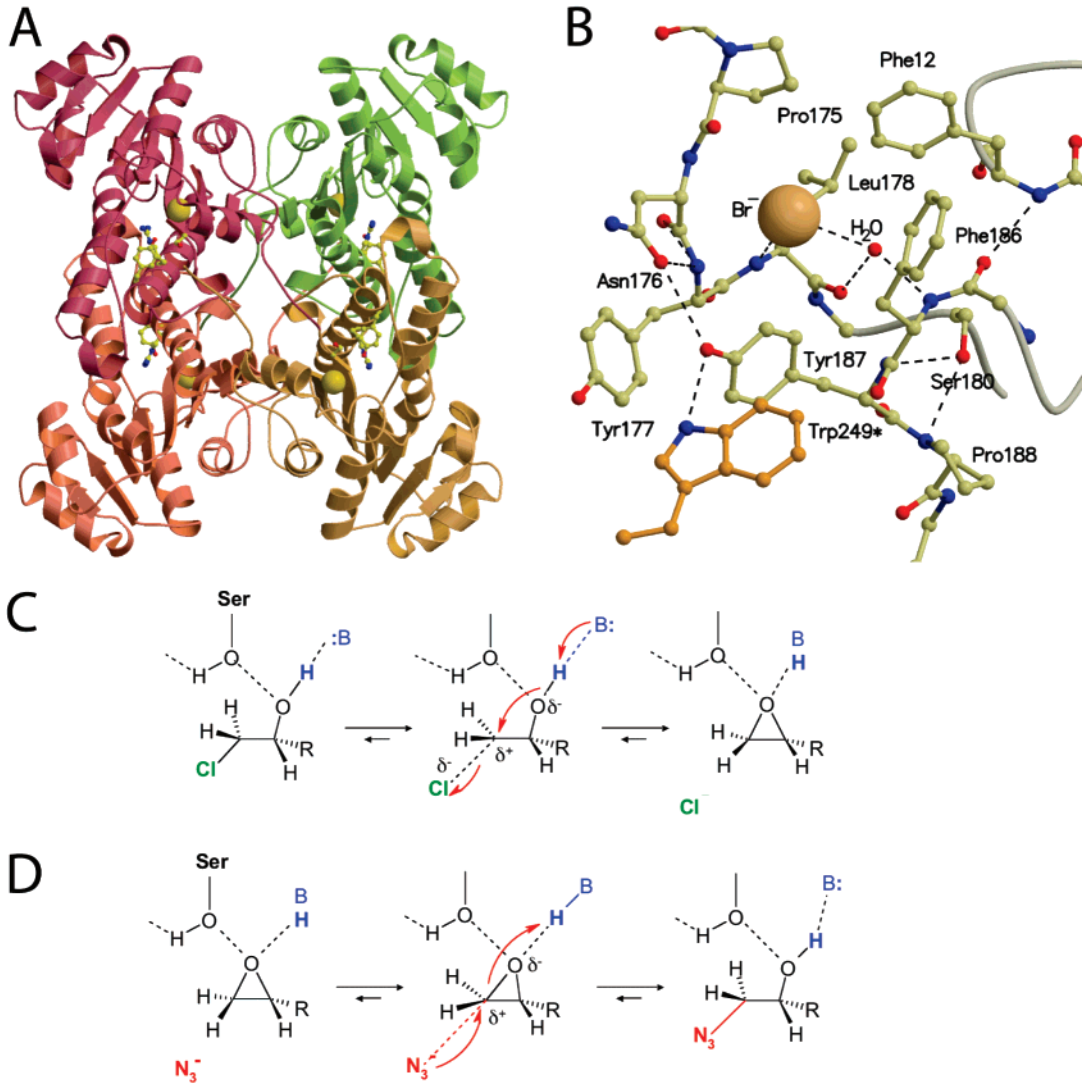

Figure 1. (A) Tetrameric structure of halo alcohol dehalogenase.[7] The Ser-Tyr-Arg catalytic triad of each monomeric subunit is shown in ball-and-stick representation. A bromide ion bound in the halide-binding site is shown as a sphere. (B) Detailed overview of the hydrophobic halide-binding site with a bound bromide ion.[7] Trp249* is contributed by an opposite monomer in the tetramer. (C) Schematic representation of the catalytic mechanism of the dehalogenation reaction catalyzed by HheC. The catalytic base tyrosine (B^-) takes up a proton from the hydroxyl group of the aromatic halo alcohol, which concurrently substitutes the chlorine, thereby producing the corresponding epoxide and a chloride ion. (D) Schematic representation of the catalytic mechanism of the epoxide ring opening reaction catalyzed by HheC. At low pH, the tyrosine (BH) donates a proton to the oxygen atom of the epoxide ring, with the concurrent attack of a bound nucleophile on its Cβ carbon atom, thereby producing the corresponding (*R*)-azido alcohol.

on the weaker binding and lower reactivity of (*S*)-pNSHH.[12] Mutagenesis experiments further showed that substitution of the side chain of Trp139 by the smaller phenylalanine side chain results in a complete loss of enantioselectivity of the enzyme for pNSHH.[13] Intriguingly, the nucleophilic ring opening reaction of racemic *para*-nitrostyrene oxide (pNSO) as well as *para*-chlorostyrene oxide[8] by azide only results in conversion of (*R*)-pNSO, but not of (*S*)-pNSO, not even when (*R*)-pNSO has been fully converted.[14] Unfortunately, a detailed kinetic analysis of this latter reaction has not been possible due to the low solubility of the epoxide in water (<2 mM).

To gain insight into the molecular basis of the high enantioselectivity of HheC in nucleophilic ring opening reactions, we crystallized the enzyme in the presence of purified enantiomers of pNSO. Here we show that both (*R*)- and (*S*)-pNSO bind in a nearly identical way in the active site of HheC, but with the crucial difference that (*S*)-pNSO adopts a nonproductive binding mode. Thermodynamic integration (TI) calculations indicate that the difference in free energy between the observed (*R*) and (*S*) bound states is small, suggesting comparable binding affinities of HheC for the two enantiomers. These results indicate that the high enantioselectivity of HheC in nucleophilic ring opening reactions of aromatic epoxides by azide is caused by the nonproductive binding of the unfavored (*S*)-enantiomer. This work thus represents a rare opportunity to explain the enantioselectivity of an enzymatic reaction by comparison of crystallographic data on the binding of both the favored and unfavored enantiomers.

Experimental Section

Purification and Crystallization. Halo alcohol dehalogenase HheC was purified and crystallized as described in the literature.[5,7,15] Sulfuric

(12) Tang, L.; Lutje Spelberg, J. H.; Fraaije, M. W.; Janssen, D. B. *Biochemistry* **2003**, *42*, 5378−5386.
(13) Tang, L.; van Merode, A. E. J.; Lutje Spelberg, J. H.; Fraaije, M. W.; Janssen, D. B. *Biochemistry* **2003**, *42*, 14057−14065.
(14) Lutje Spelberg, J. H. University of Groningen, Groningen, The Netherlands. Personal communication, 2004.

Table 1. Data Collection and Refinement Statistics

data statistics	HheC/H_2O/(*R*)-pNSO	HheC/H_2O/(*S*)-pNSO
space group	*C*2	$P2_12_12_1$
No. tetramers/ASU[a] (chains/ASU)	1 (4)	4 (16)
unit cell (Å, deg)	$a = 146.4$	$a = 118.8$
	$b = 72.0$	$b = 293.6$
	$c = 97.4$	$c = 146.7$
	$\alpha = 90$	$\alpha = \beta = \gamma = 90$
	$\beta = 92.9$	
	$\gamma = 90$	
resolution (Å)	35−1.7	35−1.9
R_{sym} (%) overall (outer shell)[b]	9.6 (47.7)	8.0 (25.8)
completeness (%) overall (outer shell)	99.1 (95.6)	90.7 (92.3)
I/σ overall (outer shell)	5.9 (2.2)	14.5 (3.5)
reflections total (unique)	890 863 (110 688)	5 753 736 (313 025)
refinement		
total atoms/water	8630/895	28 976/3298
R/R_{free}[c]	20.2/23.0	21.0/24.2
rmsd bond (Å)/angles (deg)	0.004/1.32	0.006/1.36
rmsd B (Å^2) (main chain/side chain)	0.89/1.34	0.95/1.59
Ramachandran plot (%)		
favored	85.9	85.9
allowed	12.8	12.1
generously allowed	1.3	2.0
disallowed	0.0	0.0

[a] ASU, asymmetric unit [b] $R_{sym} = \sum|I - <I>|/\sum I$, where I is the observed intensity and $<I>$ is the average intensity. [c] $R = R$ based on 95% of the data used in refinement. $R_{free} = R$ based on 5% of the data withheld for the cross-validation test.

acid was used to prepare the buffers to ensure that no halide ions were present in the crystallization solutions. The protein concentration of the stock solution for crystallization was 7.5 mg/mL.

Crystals of a HheC/H_2O/(*R*)-pNSO complex were obtained by cocrystallization. A solution of (*R*)-pNSO (ee = 98 ± 0.5%)[9] solubilized in a small amount of dimethyl sulfoxide (<1 μL) was added to 50 μL of the purified and dialyzed protein solution to a final concentration of 10 mM. After equilibrating the protein solution for 30 min, we removed undissolved (*R*)-pNSO by centrifugation at 3000*g*. Hanging drops with a total volume of 3 μL were prepared by mixing 1.5 μL of the protein−substrate mixture with 1.5 μL of the standard reservoir solution. Plate-shaped crystals with space group *C*2 appeared in a few days and diffracted to 1.7 Å. They contained four HheC monomers per asymmetric unit.

A HheC/H_2O/(*S*)-pNSO complex was obtained by the same protocol as described for the HheC/H_2O/(*R*)-pNSO complex, using a final concentration of 10 mM of enantiopure (*S*)-pNSO (ee = 99 ± 0.5%).[9] Bipyramidal crystals appeared in a few days and diffracted to 1.9 Å. They had space group $P2_12_12$ and contained 16 HheC monomers in the asymmetric unit.

Data Collection and Refinement. Diffraction data were collected at 100 K using an X-ray wavelength of 0.93 Å at the ID14-1 and ID14-2 beam lines of the ESRF in Grenoble. All data processing was done using DENZO and SCALEPACK,[16] while refinements were done with the CNX program suite (Accelrys, Inc., San Diego, CA). Initial phases were obtained from rigid body fitting in CNX. Model coordinates for the substrate molecules were obtained by building and energy-minimizing them with the program QUANTA (Accelrys, Inc.). Parameter and topology files for these compounds were obtained from the HIC-Up server.[17] When needed, the protein models were manually rebuilt in QUANTA (Accelrys, Inc.) and Xtalview.[18] Data collection and refinement statistics are summarized in Table 1. Figures of molecular models were prepared using MOLSCRIPT[19] and RASTER3D,[20] unless otherwise stated. The coordinates and structure factor amplitudes of the (*R*)-pNSO and (*S*)-pNSO complexes of the halo alcohol dehalogenase HheC have been deposited in the Protein Data Bank under accession number 1ZMT and 1ZO8, respectively.

Computational Techniques. The structure of the HheC/H_2O/(*R*)-pNSO complex was used as the starting structure for molecular dynamics (MD) calculations. To limit the amount of data analysis, the bound epoxide in one of the four active sites of the tetrameric enzyme was retained, whereas the other three epoxides were replaced by water molecules. The tetrameric enzyme and the single bound epoxide were hydrated in a box containing ∼27 000 simple point charge water molecules.[21] Sixteen Na^+ ions were added to balance the total charge of the system. The enzyme and epoxide were described using the GROMOS96 (43a2) force field,[22,23] in which aliphatic hydrogen atoms are treated as united atoms, together with the carbon atom to which they are attached. The bond and bond-angle parameters for the epoxide group were taken from previously reported molecular dynamics simulations of epoxides.[24] The charges of the epoxide were determined from ab initio quantum mechanical calculations using the Hartree−Fock approximation, resulting in charges of −0.46 on the oxygen atom and 0.23 on the Cα and Cβ atoms. The charges of ionizable groups of the protein were appropriate for pH 7. Arg and Lys residues were protonated, and Asp and Glu residues were negatively charged. Protonation of histidine residues was based on local interactions.

All simulations were performed using the GROMACS package version 3.0[25−27] in a periodic dodecahedral box. Nonbonded interactions were evaluated using a twin-range cutoff. Interactions within the short-range cutoff (0.9 nm) were evaluated every step, whereas interactions within the long-range cutoff (1.4 nm) were updated every five steps, together with the pair list. To correct for the neglect of electrostatic interactions beyond the 1.4 nm cutoff, a reaction field (RF) correction with $\epsilon_{RF} = 78.0$ was used. To maintain a constant temperature and pressure, a Berendsen thermostat[27] was applied. The protein, epoxide, solvent, and ions were independently coupled to a temperature bath (25 °C) with a coupling time of 0.1 ps. The pressure was held at 1 bar, with a coupling time of 0.5 ps. The isothermal compressibility was 4.6×10^{-5} bar^{-1}.[28] The time step was 0.002 ps. The bond lengths and bond angle of water were restrained using the SETTLE algorithm.[29] Bond lengths within the protein were constrained using the LINCS algorithm.[30]

A 2-ns simulation of the HheC/H_2O/(*R*)-pNSO complex was performed to equilibrate the structure of the enzyme. The enzyme retains its overall conformation during the simulation, having an average rmsd of 0.15 Å for all the backbone atoms compared to the crystal structure. Furthermore, the bound (*R*)-pNSO molecule retains its hydrogen bonds with the catalytic residues Ser132 and Tyr145.

(15) de Jong, R. M.; Rozeboom, H. J.; Kalk, K. H.; Tang, L.; Janssen, D. B.; Dijkstra, B. W. *Acta Crystallogr., Sect. D* **2002**, *58*, 176−178.
(16) Otwinowski, Z.; Minor, W. *Methods Enzymol.* **1997**, *276*, 307−326.
(17) Kleywegt, G. J.; Jones, T. A. *Acta Crystallogr., Sect. D* **1998**, *54*, 1119−1131.
(18) McRee, D. E. *J. Struct. Biol.* **1999**, *125*, 156−165.
(19) Kraulis, P. J. *J. Appl. Crystallogr.* **1991**, *24*, 946−950.
(20) Merritt, E. A.; Bacon, D. J. *Methods Enzymol.* **1997**, *277*, 505−524.
(21) Berendsen, H. J. C.; Postma, J. P. M.; van Gunsteren, W. F.; Hermans, J. In *Intermolecular Forces*; Pullman, B., Ed.; Reidel: Dordrecht, The Netherlands, 1981; pp 131−137.
(22) van Gunsteren, W. F.; Billeter, S. R.; Eising, A. A.; Hünenberger, P. H.; Krüger, P.; Mark, A. E.; Scott, W. R. P.; Tironi, I. G. *Biomolecular simulation: GROMOS96 Manual and User Guide*; Hochschulverlag AG an der ETH Zürich: Zürich, Switzerland, 1996.
(23) Schuler, L. D.; van Gunsteren, W. F. *Mol. Simul.* **2000**, *25*, 301−319.
(24) Schiott, B.; Bruice, T. C. *J. Am. Chem. Soc.* **2002**, *124*, 14558−14570.
(25) Berendsen, H. J. C.; van der Spoel, D.; van Drunen, R. *Comput. Phys. Commun.* **1995**, *91*, 43−56.
(26) van der Spoel, D.; van Buuren, A. R.; Apol, E.; Meulenhoff, P. J.; Tieleman, D. P.; Sijbers, A. L. T. M.; Hess, B.; Feenstra, K. A.; Lindahl, E.; van Drunen, R.; Berendsen, H. J. C. *Gromacs User Manual*, version 3.0; University of Groningen: Groningen, The Netherlands, 2001 (http://www.gromacs.org).
(27) Lindahl, E.; Hess, B.; van der Spoel, D. *J. Mol. Model.* **2001**, *7*, 306−317.
(28) Berendsen, H. J. C.; Postma, J. P. M.; van Gunsteren, W. F.; DiNola, A.; Haak, J. R. *J. Chem. Phys.* **1984**, *81*, 3684−3690.
(29) Miyamoto, S.; Kollman, P. A. *J. Comput. Chem.* **1992**, *13*, 952−962.
(30) Hess, B.; Bekker, H.; Berendsen, H. J. C.; Fraaije, J. G. E. M. *J. Comput. Chem.* **1997**, *18*, 1463−1472.

Free Energy Calculations. The difference in Gibbs free energy between two states of a system was determined using the coupling parameter approach in conjunction with the TI formula:[31]

$$\Delta G_{A\rightarrow B} = \int_{\lambda_A}^{\lambda_B} \left\langle \frac{\partial H(\lambda)}{\partial \lambda} \right\rangle_{\lambda} d\lambda \quad (1)$$

In this approach, the Hamiltonian H is made a function of a coupling parameter, λ. The λ-dependence of the Hamiltonian defines a pathway, that which connects two states A and B of the system. To solve eq 1, the ensemble average at a number of discrete λ-points was obtained by performing separate simulations for each chosen λ-point, and the integral was determined numerically.

The change in Gibbs free energy resulting from the change of (*R*)-pNSO to (*S*)-pNSO was achieved by gradually mutating the epoxide oxygen atom of (*R*)-pNSO into a carbon atom and the Cβ atom into an oxygen atom. The interchange of the epoxide oxygen and Cβ atom thus provides a minimal way to invert the stereocenter of the epoxide Cα atom. Only bonded and nonbonded interactions were mutated during the calculations. The masses of the atoms were not altered. The nonbonded interactions between states A and B were interpolated using a soft-core potential,[32] as implemented in the GROMACS simulation package.[27,33]

The TI calculations were started from the equilibrated structure. Separate simulations were performed at 21 discrete λ-points from $\lambda = 0$ (state A) to $\lambda = 1$ (state B). At each λ-point, the data for the complex were collected for 180 ps. To obtain the relative Gibbs binding energy $\Delta\Delta G_{A\rightarrow B}$, the average $\langle \partial H(\lambda)/\partial\lambda \rangle_{\lambda}$ at each λ-point (eq 1) was integrated using the trapezoidal method. The error in $\langle \partial H(\lambda)/\partial\lambda \rangle_{\lambda}$ was estimated using a block averaging procedure,[34,35] and the errors were integrated to give the total error in $\Delta\Delta G_{A\rightarrow B}$.

Results and Discussion

Structure of the HheC/H_2O/(*R*)-pNSO Complex at 1.8 Å Resolution. Cocrystallization in the presence of the favored epoxide (*R*)-pNSO resulted in a HheC/H_2O/(*R*)-pNSO complex, with a water molecule occupying the halide-binding site (Figure 2A). (*R*)-pNSO binds in the active site of HheC with hydrogen bonds of approximately 2.9 Å with the side chain oxygen atoms of the catalytic residues Ser132 and Tyr145 (Figure 2B). The water molecule in the halide-binding site is positioned at approximately 3.1 Å from the Cβ atom of the epoxide ring of (*R*)-pNSO. A nucleophile such as azide bound at this position would be in a productive position for an epoxide ring opening attack.

Structure of an HheC/H_2O/(*S*)-pNSO Complex at 1.9 Å Resolution. Cocrystallization of HheC with the unfavored (*S*)-enantiomer of pNSO yielded crystals of a HheC/H_2O/(*S*)-pNSO complex that diffracted to 1.9 Å resolution. Electron density for a pNSO molecule is present in the active sites of all 16 molecules in the asymmetric unit (Figure 2C), although not well-defined in all of them. This electron density was very similar to the electron density observed in the HheC/H_2O/(*R*)-pNSO structure, indicating that the aromatic ring and epoxide group of (*R*)- and (*S*)-pNSO are located at similar positions. A water molecule occupies the halide-binding site.

To obtain an unbiased view of the interactions of the epoxide moieties of both enantiomers, we modeled the substrate as *para*-nitrophenylcyclopropane and refined the HheC structure with the bound *para*-nitrophenylcyclopropane against the diffraction data of both the HheC/H_2O/(*R*)-pNSO and HheC/H_2O/(*S*)-pNSO complexes. This strategy resulted in a clear discrimination between the species bound in the two complexes. When refined against the HheC/H_2O/(*R*)-pNSO data, the cyclopropane ring moved close enough to the Ser132 and Tyr145 side chain oxygen atoms to be compatible with a hydrogen bonding interaction of the epoxide oxygen atom of (*R*)-pNSO with the catalytic residues. Refinement against the HheC/H_2O/(*S*)-pNSO data, however, moved the cyclopropane ring away from the catalytic residues but near enough to the water molecule in the halide-binding site for a hydrogen bonding interaction between the water molecule and the epoxide oxygen of (*S*)-pNSO. This result was further corroborated by refinement of the (*R*)-pNSO and (*S*)-pNSO complexes against the (*R*)-pNSO and (*S*)-pNSO diffraction data, which resulted in good hydrogen bonding interactions of the (*R*) and (*S*) epoxides with the catalytic residues and the water molecule, respectively.

This refinement strategy confirms that cocrystallization of HheC with enantiopure (*R*)- and (*S*)-pNSO resulted in HheC/H_2O/(*R*)-pNSO and HheC/H_2O/(*S*)-pNSO complexes, respectively. The epoxide rings of both enantiomers occupy similar positions in the active site of HheC, but with the crucial difference that the epoxide oxygen of (*R*)-pNSO is hydrogen bonded to the hydroxyl groups of Ser132 and Tyr145, whereas the oxygen atom of (*S*)-pNSO forms a hydrogen bond with the water molecule in the halide-binding site. Similarly, the epoxide Cβ atom of (*R*)-pNSO is directed toward the water molecule in the halide-binding site, and the epoxide Cβ atom of (*S*)-pNSO has van der Waals interactions with the hydroxyl groups of Ser132 and Tyr145. Therefore, (*R*)-pNSO is bound in a way similar to that observed in the previously described HheC/Cl^-/(*R*)-styrene oxide ((*R*)-SO) complex (Figure 2D),[7] whereas (*S*)-pNSO is bound in a nonproductive way (Figure 2E). The aromatic ring of both pNSO enantiomers is fixed by the side chains of Trp139 and Phe186. Mutation of Trp139 to a smaller residue enlarges the binding pocket and gives more positional freedom to the aromatic ring of pNSHH or pNSO substrate. This offers a plausible explanation for the loss of enantioselectivity of HheC toward aromatic substrates upon mutation of W139.[13]

Calculations of the Relative Gibbs Binding Energy of (*R*)- and (*S*)-pNSO. To further substantiate the nonproductive binding of the (*S*)-enantiomer of pNSO, we calculated the relative Gibbs binding energy ($\Delta\Delta G_{(R)\rightarrow(S)}$) of the pNSO enantiomers from thermodynamic integration calculations. $\Delta\Delta G_{(R)\rightarrow(S)}$ of the HheC-bound states of (*R*)- and (*S*)-pNSO, with a water molecule in the halide-binding site, was evaluated using the thermodynamic cycle shown in Figure 3A.

No simulations of the free epoxide compounds were necessary, as the work required to mutate (*R*)-pNSO into (*S*)-pNSO in water is zero. Thus the relative Gibbs binding energy, $\Delta\Delta G_{(R)\rightarrow(S)}$, corresponds to the work done to (nonphysically) mutate (*R*)-pNSO into (*S*)-pNSO while bound to HheC,

(31) Mark, A. E. In *Encyclopedia of Computational Chemistry*; von Ragué Schleyer, P., Ed.; Wiley: New York, 1998; pp 1070−1083.
(32) Beutler, T. C.; Mark, A. E.; van Schaik, R. C.; Geber, P. R.; van Gunsteren, W. F. *Chem. Phys. Lett.* **1994**, *222*, 529−539.
(33) Villa, A.; Mark, A. E. *J. Comput. Chem.* **2002**, *23*, 548−553.
(34) Bishop, M.; Frinks, S. *J. Chem. Phys.* **1987**, *87*, 3675−3676.
(35) Allen, M. P.; Tildesley, D. J. *Computer Simulations of Liquids*; Oxford Science Publications: Oxford, 1987.
(36) Fersht, A. R.; Shi, J. P.; Knill-Jones, J.; Lowe, D. M.; Wilkinson, A. J.; Blow, D. M.; Brick, P.; Carter, P.; Waye, M. M.; Winter, G. *Nature* **1985**, *314*, 235−238.
(37) Shue, S.-Y.; Yang, D.-Y.; Selzle, H. L.; Schlag, E. W. *Proc. Natl. Acad. Sci. U.S.A.* **2003**, *100*, 12683−12687.
(38) Brünger, A. T.; Adams, P. D.; Rice, L. M. *Structure* **1997**, *5*, 325−336.

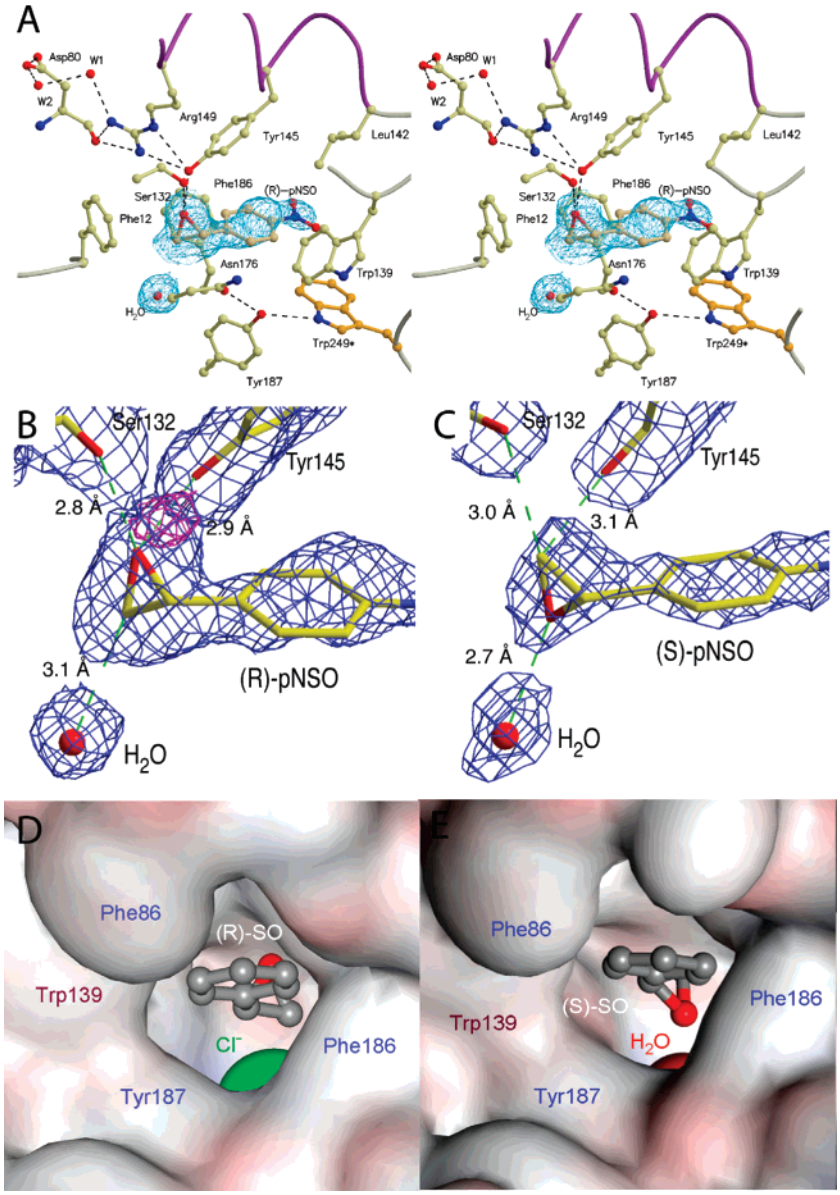

Figure 2. (A) Overview of the active site of the HheC/H_2O/(*R*)-pNSO complex. The oxygen atom of the epoxide ring of (*R*)-pNSO is hydrogen bonded to Ser132 and Tyr145 of the catalytic triad. Arg149 is hydrogen bonded to Tyr145 and forms a proton relay system with two buried water molecules and the side chain of the partly solvent exposed Asp80. A water molecule, instead of a halide ion, occupies the halide-binding site. Portions of a $2F_o - F_c$ simulated annealing electron density omit map are shown,[38] contoured at 1σ and covering the bound (*R*)-pNSO and a water molecule. Residues are shown in ball-and-stick representation. Hydrogen bonds are indicated by black dashed lines. (B) Detailed view of one of the active sites in the HheC/H_2O/(*R*)-pNSO complex with a dark colored σA-weighted $2F_o - F_c$ electron density map at 1.7 Å resolution covering the water molecule and (*R*)-pNSO molecule contoured at 1.2 σ. The pink colored mesh represents the σA-weighted $F_o - F_c$ electron density map contoured at 3.0 σ, which was obtained after refining the structure with *para*-nitrophenylcyclopropane. The refined distances between the different atoms are shown in Å. (C) Detailed view of one of the active sites in the HheC/H_2O/(*S*)-pNSO complex with a dark colored σA-weighted $2F_o - F_c$ electron density map at 1.9 Å resolution covering the water molecule and (*S*)-pNSO molecule contoured at 1.2 σ. (D) Surface representation of part of the active site cavity of HheC with bound dehalogenation products (*R*)-SO and chloride.[7] The oxygen atom of the epoxide ring is hydrogen bonded to the side chain oxygen atoms of the catalytic residues Ser132 and Tyr145 in the upper part of the cavity. (E) Surface representation of part of the active site cavity of HheC with a bound (*S*)-pNSO molecule and a water molecule occupying the halide-binding site. The nitro group of the molecule has been omitted for clarity. The epoxide oxygen atom is hydrogen bonded to the water molecule, whereas the Cβ atom has van der Waals interactions with the side chain oxygen atoms of Ser132 and Tyr145.

$\Delta G_{(R)-\mathrm{pNSO}-(S)-\mathrm{pNSO}}$. This transformation is accomplished by the stepwise transformation of the Cβ and O atoms of the epoxide ring into each other. The relative Gibbs binding energy is estimated from 21 independent MD simulations at different λ-values. For each simulation, the derivative $\partial H(\lambda)/\partial\lambda$ was averaged over 180 ps. The numerical integration of the resulting free energy profile resulted in a relative Gibbs binding energy of $+4.7 \pm 3.1$ kJ/mol ($+1.1 \pm 0.7$ kcal/mol) when mutating (*R*)- into (*S*)-pNSO in the complex, similar to the average free energy loss upon rupture of a single peptide hydrogen bond in water.[36,37] This relative Gibbs binding energy can in principle be used to estimate the relative binding constants for the two enantiomers, but the large error in the outcome precludes an accurate estimation.

The small difference in Gibbs binding energy is in good agreement with the ability of HheC to accommodate both enantiomers in the active site. During the simulations, the position of the aromatic side chain remained approximately the

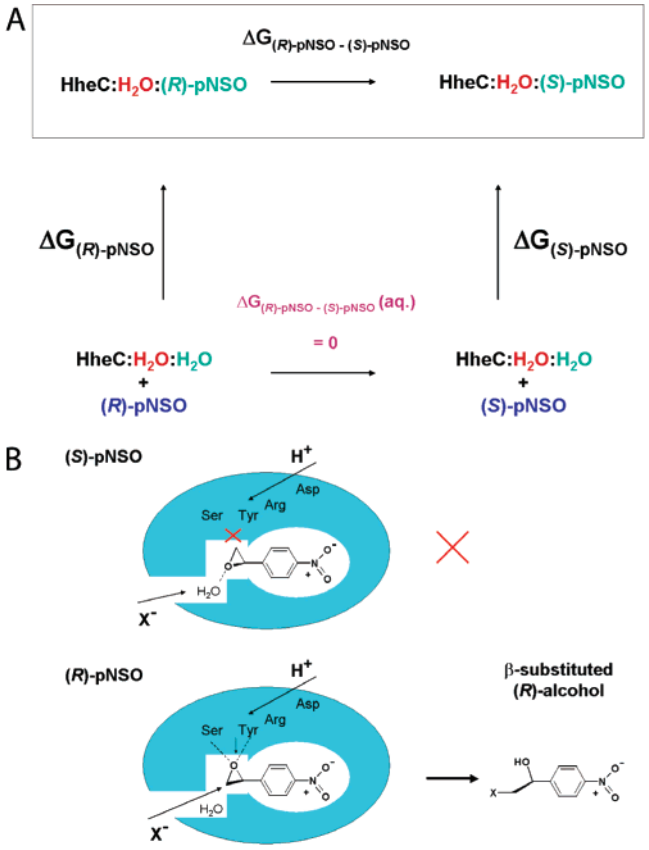

Figure 3. (A) Schematic representation of the thermodynamic cycle that was used in the TI calculations, where $\Delta G_{(R)-\text{pNSO}}$ and $\Delta G_{(S)-\text{pNSO}}$ are the binding Gibbs energy of the (*R*)- and (*S*)-pNSO to HheC, respectively, and $\Delta G_{(R)-\text{pNSO}-(S)-\text{pNSO}}$ is the work required to mutate the (*R*) into (*S*) in HheC ($\Delta G_{(R)-\text{pNSO}-(S)-\text{pNSO}}$) and in water ($\Delta G_{(R)-\text{pNSO}-(S)-\text{pNSO}}$ (aq)). The boxed part is the only part that needs to be evaluated. (B) Schematic representation of the binding and catalysis of (*S*)- and (*R*)-pNSO in the active site of HheC. In contrast to the (*R*)-enantiomer of pNSO, the (*S*)-enantiomer binds in a nonproductive conformation that does not permit protonation of the epoxide O atom and the concurrent attack of its Cβ atom by a nucleophilic anion (X^-) in the halide-binding site. Therefore, only the (*R*)-enantiomer can be converted to its corresponding β-substituted alcohol.

same, fixing the location of the epoxide ring, which in both enantiomers of pNSO fits snugly in the active site. Therefore, the difference in Gibbs binding energy is unlikely to depend on changed van der Waals interactions, but rather on the reduced number of hydrogen bonds that (*S*)-pNSO is able to make (two hydrogen bonds with the catalytic residues in the (*R*)-pNSO complex versus one hydrogen bond with the water molecule in the halide binding site in the (*S*)-pNSO complex). Moreover, during the simulations, (*R*)-pNSO retains a productive binding mode in the active site of HheC, while (*S*)-pNSO does not. Although the epoxide ring of (*S*)-pNSO is much more mobile in the active site, the binding of the *p*-nitrophenyl ring prevents the O and Cβ atoms to align properly for the concurrent protonation by the tyrosine and nucleophilic attack by the water molecule in the halide-binding site.

Conclusions

We have presented a combined crystallographic and computational analysis of the binding of (*R*)- and (*S*)-enantiomers of the aromatic pNSO epoxides to the halo alcohol dehalogenase HheC, with a water molecule rather than a halide ion occupying the halide-binding site. The crystallographic data show that both enantiomers bind with their aromatic side chains in a very similar conformation in the active site, but with the crucial difference that the oxygen and Cβ atom of the epoxide ring are inverted. The oxygen atom of the epoxide ring of the bound (*S*)-enantiomer is in the wrong position to accept a proton from the catalytic residue Tyr145, and its Cβ atom is too far away for attack by a nucleophile. The nonproductive orientation of the epoxide ring in the active site thus prevents the enzymatic azidolysis reaction of (*S*)-pNSO. Calculation of the relative Gibbs binding energy of the (*R*)-pNSO and (*S*)-pNSO bound states suggests that the difference in free energy of binding of the two enantiomers is relatively small ($\Delta\Delta G_{(R)\rightarrow(S)} = +4.7 \pm 3.1$ kJ/mol).

On the basis of these results, we propose that the high enantioselectivity of HheC toward aromatic epoxides in the epoxide ring opening reaction by azide is mainly determined by the inability of (*S*)-pNSO to form a productive complex in the active site, rather than by a large difference in binding affinity of the different enantiomers (Figure 3B). The unfavored (*S*)-enantiomer likely has less affinity for the substrate-binding site of HheC and thus has higher K_M values than the corresponding (*R*)-enantiomer. However, the inability of HheC to convert the (*S*)-enantiomer is best explained by the nonproductive binding mode of this compound, which indicates that the k_{cat} will be much lower for the (*S*)-enantiomer than for the (*R*)-enantiomer. This is in sharp contrast with the corresponding dehalogenation reaction, in which weaker binding of the unfavored (*S*)-enantiomer governs the enantioselectivity and k_{cat} values are only slightly reduced.

Acknowledgment. We thank Jeffrey Lutje Spelberg for providing optically pure (*R*) and (*S*)-pNSO. This research was supported by The Netherlands Foundation of Chemical Research (CW) with financial aid from The Netherlands Foundation for Scientific Research (NWO).

JA0531733